EAI Endorsed Transactions
on Energy Web
Research Article EAI.EU

Optimization of operation and dispatching of integrated energy system based on Nash bargaining model

Yuwei Wang[1,*], Yu Shi[1], Rui Zhou[2], Yang Liu[3] and Xin Wang[4]

[1]State Grid Jilin Electric Power Co., Ltd. Economic and Technical Research Institute, 1427 Pingquan Road, Changchun City, Jilin Province, China
[2]State Grid Jilin Electric Power Company Limited, 10388 Renmin Street, Changchun City, Jilin Province, China
[3]Office of State Grid Jilin Electric Power Co., Ltd, 10388 Renmin Street, Changchun City, Jilin Province, China
[4]School of Materials Science and Engineering, Jilin University, 5988 Renmin Avenue, Changchun City, Jilin Province, China

Abstract

INTRODUCTION: With the growing energy demand, the Integrated Energy System (IES) has attracted wide attention for its high efficiency, economy, and environmental friendliness. Compared with traditional energy systems, IES realizes multi-energy complementarity through the coupling of electricity, heat, gas, and hydrogen. International research focuses on market mechanisms, renewable energy integration, and digital technologies, but issues such as wind-solar output uncertainty and fair benefit distribution in multi-party cooperation remain to be addressed.
OBJECTIVES: This paper aims to construct an optimal operation and dispatching model for IES integrating renewable energy, gas-fired thermal power plants, and carbon capture power plants, handle wind-solar output uncertainty, and design a fair benefit distribution mechanism based on Nash bargaining theory to balance economy and environmental protection and maintain cooperation enthusiasm. Compared with traditional methods such as the Shapley value, which allocates benefits based on marginal contributions, the Nash bargaining approach emphasizes fair negotiation outcomes and better accommodates differences in participants' investments, risks, and bargaining power.
METHODS: 1. Establish an IES mathematical model covering core equipment such as wind turbines, PV panels, P2G devices, hydrogen storage tanks, and CHP units. 2. Use KDE to fit wind-solar output marginal distribution, construct a joint probability model with Frank Copula function, and generate typical scenarios via K-means clustering. 3. Adopt a two-stage optimization: first, use mixed-integer linear programming to calculate the total alliance revenue; second, apply symmetric/asymmetric Nash bargaining models for benefit distribution.
RESULTS: Based on Liaoning regional grid data, the tripartite alliance reduces system operation cost by approximately 22% and increases renewable energy consumption rate by 18% compared with independent operation. P2G and hydrogen storage realize time-shifting energy transfer, and CHP units adjust output to reduce costs. The Nash bargaining-based benefit distribution meets individual and collective rationality, with all parties' revenues exceeding independent operation.
CONCLUSION: The IES model integrating hydrogen storage, P2G, and carbon capture enhances multi-energy complementarity and time-shifting regulation capacity. The Nash bargaining mechanism ensures fair surplus distribution, providing theoretical and methodical references for multi-party IES collaborative operation.

Keywords: Integrated energy system; Multi-energy complementarity; Nash bargaining; Benefit distribution; Optimal dispatch

Received on 15 December 2025, accepted on 15 January 2026, published on 27 February 2026

doi: 10.4108/ ew.11358

*Corresponding author. Email:1370804475@qq.com

1. Introduction

The academic community has extensively investigated the optimal operation of integrated energy systems (IES), with recent advancements focusing on system modeling, optimization algorithms, and market mechanisms.

Internationally, research has emphasized market mechanisms, high renewable energy integration, and digital technologies. For instance, European demonstration projects such as Denmark's Bornholm Island and Germany's E-Energy have achieved high renewable penetration through blockchain and multi-agent systems[1–2]. In the United States, the National Renewable Energy Laboratory (NREL) applied the alternating direction method of multipliers (ADMM) for multi-microgrid coordination[3], while Australia's Tasmanian project explored wind–solar–hydrogen integration for off-grid applications. Digitalization is also advancing rapidly, with the European Union promoting blockchain applications and General Electric developing digital twin platforms[4]. These international efforts benefit from mature markets, advanced power-to-X (P2X) technologies, and supportive policies, offering valuable insights for IES development in China.

Building on these developments, this paper establishes a mathematical model for an IES that incorporates renewable energy, gas-fired power plants, and carbon capture power plants, accurately characterizing the coupling and conversion relationships among electricity, heat, natural gas, and hydrogen. To address the uncertainty and correlation of wind and photovoltaic power output, a joint probability model is constructed using the Frank Copula function, and typical scenarios are generated via K-means clustering. An optimal dispatch model aimed at maximizing the total alliance benefit is developed. Furthermore, the Nash bargaining theory is introduced to design a fair and efficient benefit distribution mechanism for the cooperative surplus. A case study based on real-world data from a regional grid in Liaoning Province, China, validates the model's effectiveness in enhancing system economics, promoting renewable energy utilization, and ensuring equitable benefit allocation.

The main innovations of this work are threefold: (1) establishing a comprehensive IES model integrating renewable energy, gas-fired thermal power, and carbon capture plants for coordinated scheduling of multi-energy flows; (2) employing the Frank Copula and K-means methods to generate typical scenarios addressing wind–solar uncertainty and correlation; and (3) introducing the Nash bargaining theory for the first time into the cooperative surplus allocation mechanism, ensuring fairness and cooperation enthusiasm among all participants. Unlike the Shapley value that relies on marginal contributions for benefit division and neglects heterogeneous bargaining power, Nash bargaining emphasizes negotiation-oriented equity and can flexibly reflect differences in participants' investment scales, risk levels, and technical contributions.

2. Integrated energy system modeling

2.1. Integrated energy system structure

The structure of the integrated energy system studied in this paper is shown in Figure.1. The main structure of the system is a new energy power plant, which includes wind power generation and photovoltaic power generation units and is the main source of clean energy for the system[5]; the gas-fired thermal power plant is equipped with combined heat and power (CHP) units, which can provide both electricity and heat by burning gas; the P2G equipment includes equipment such as electrolyzers, methane reactors and hydrogen storage tanks, which can store the surplus electricity of the system in the form of hydrogen or natural gas; the gas boiler serves as a backup heat source and provides supplementary heat when the CHP fails to supply sufficient heat; the carbon capture power plant's CCS equipment provides CO2 to the P2G equipment; the energy network includes the power grid, heat network and gas network, which realize the transmission and distribution of energy.

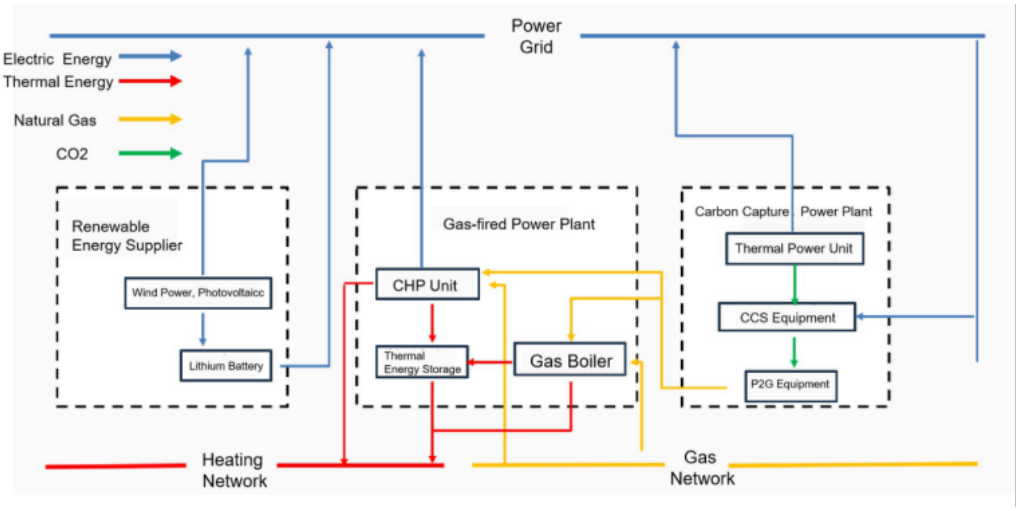

Figure 1. Integrated energy system structure

2.2. Mathematical model of integrated energy system

2.2.1. Wind power generation and photovoltaic power plant models

Wind power plants convert wind energy into electricity through turbine rotation. They are categorized as onshore (land-based, technologically mature) or offshore (higher energy stability but greater construction and maintenance costs). Key advantages include zero carbon emissions and resource abundance, while disadvantages involve intermittency due to wind variability, requiring energy storage and control systems for stable operation.

Photovoltaic (PV) power plants generate electricity via the photovoltaic effect. Centralized PV stations are large-scale installations in sunny areas, feeding electricity into the grid, whereas distributed PV systems (e.g., rooftop solar) enable local generation and consumption, reducing transmission losses. However, PV generation is highly weather-dependent, posing challenges for consistent power supply [6]. For both wind and PV power generation, the absorption power must be a non-negative value not exceeding the rated generation capacity of the unit.

$$0 \le P_{\mathrm{wt}} \le S_w \tag{1}$$

In the formula: P_{wt} is the power consumption for the fan, S_w Fan power.

The absorption power of the photovoltaic should be less than the power generated by the photovoltaic power generation, and it is also a positive number.

$$0 \le P_{pv} \le S_p \tag{2}$$

In the formula: P_{pv} is Photovoltaic absorption power, S_p For photovoltaic power.

Wind and solar curtailment penalty cost: Set the penalty cost per unit power of wind and solar curtailment, calculate the sum of penalty costs, and obtain the penalty cost of wind and solar curtailment.

$$CQ = sum(beta1(S_w - P_{wt}) + beta2(S_p - P_{pv})) \tag{3}$$

In the formula: $beta1$ is the wind curtailment penalty, $beta2$ is the penalty for abandoning the sun.

2.2.2. P2G equipment model

P2G technology converts electrical energy into gaseous fuel through electrochemical or catalytic reactions, which can be broadly divided into two stages. The first stage involves water electrolysis using renewable energy to produce hydrogen and oxygen. The second stage utilizes catalytic methanation to synthesize methane from hydrogen and carbon dioxide. In this context, P2G primarily addresses renewable energy integration by converting excess electricity from wind and solar power into methane for storage. Since both methane and hydrogen can be stored long-term, this approach effectively compensates for the limited storage duration of conventional batteries[7].

Carbon capture plants utilize P2G technology to convert electricity into natural gas, involving electrolysis for hydrogen production and methanation reactions. The electrolyzer model demonstrates electrolysis efficiency, with the P2G equipment's P2G conversion ratio being specified. Calculate the proportion of electricity consumed by P2G equipment that is converted into hydrogen.

$$V_{H2} = P_{P2G}\eta_{H2} \tag{4}$$

In the formula: η_{H2} is Electrolytic cell conversion efficiency, P_{P2G} is the power consumption of P2G electrolysis for hydrogen production, V_{H2} is the amount of hydrogen produced by the electrolytic cell.

The hydrogen production power limit is shown in the following equation.

$$V_{H2,\min} \le V_{H2} \le V_{H2,\max} \tag{5}$$

In the formula: $V_{H2,\max}$ is the maximum and minimum power of electrolytic cell hydrogen production are respectively.

Methane reactor model: Methanation efficiency, defined as the hydrogen conversion efficiency in methanation reactors, Determine the ratio of hydrogen to methane conversion in the methane reactor.

$$P_{MRg} = \eta_{ch4}P_{MRh} \tag{6}$$

In the formula: P_{MRg} is the output natural gas power for the methane reactor, P_{MRh} is the enter hydrogen power for methane reactions, η_{ch4} Methane reactor conversion efficiency.

The power generation limit is given by the following equation.

$$P_{MRg,\min} \le P_{MRg} \le P_{MRg,\max} \tag{7}$$

In the formula: $P_{MRg,\min}$, $P_{MRg,\max}$ is the minimum and maximum power output of the methane reactor is respectively.

2.2.3 Hydrogen storage tank model

Hydrogen storage systems are a critical component of the hydrogen energy industry chain, with their technological advancement directly impacting the feasibility and cost-effectiveness of hydrogen applications. The current mainstream high-pressure gaseous hydrogen storage technology employs a composite structure design featuring "metal liner + carbon fiber winding," achieving high hydrogen storage density while ensuring safety. These

storage containers utilize high-strength aluminum alloy as the liner material, with an outer layer of high-modulus carbon fiber composite material wound for reinforcement, capable of withstanding pressures up to 70MPa. To ensure operational safety, the system is equipped with intelligent monitoring devices and multiple pressure relief protection mechanisms. Its reliability has been rigorously tested through fatigue testing. With advancements in material science and manufacturing processes, the application of new composite materials continues to enhance the performance and cost-effectiveness of hydrogen storage systems, providing robust support for large-scale commercialization of hydrogen energy [8].

The hydrogen storage tank in this paper is used to balance the supply and demand of hydrogen energy and achieve the effect of peak shaving and valley filling. Its operation constraints include: charging and discharging exclusion constraint: to ensure that charging and discharging can not be carried out at the same time in principle, in order to ensure safety.

$$H_{h2dis} + H_{h2cha} \le 1 \tag{8}$$

Where: H_{h2dis} is the discharge variable of the hydrogen storage tank, and H_{h2cha} is the charging variable of the hydrogen storage tank.

Charging and discharging power constraints: Constraints on the power of hydrogen storage tank charging and discharging.

$$\begin{cases} 0 \le P_{h2cha} \le 50 H_{h2cha} \\ 0 \le P_{h2dis} \le 50 H_{h2dis} \end{cases} \tag{9}$$

Where: P_{h2dis} is the discharge power of the hydrogen storage tank, and P_{h2cha} is the charging power of the hydrogen storage tank.

2.2.4 CHP unit model

A CHP unit is an efficient multi-energy system designed based on the principle of energy cascade utilization. Its key feature is the simultaneous generation of electricity and heat through a single energy conversion process. From a thermodynamic perspective, the CHP system recovers waste heat typically lost in conventional power generation, boosting overall energy efficiency from 30-45% in traditional plants to 70-90%, thereby maximizing energy value.

From a technical implementation perspective, modern CHP units predominantly utilize gas turbines, internal combustion engines, or steam turbines as prime movers, integrated with waste heat recovery systems to form complete energy conversion chains. The gas turbine combined cycle system, owing to its flexible regulation and rapid start-up capabilities, has become the preferred configuration for regional energy stations. Meanwhile, reciprocating internal combustion engine CHP systems, leveraging their high efficiency under partial load conditions, have gained widespread adoption in distributed energy projects[9].

In terms of carbon emissions, CHP systems demonstrate 20-30% lower CO2 output than conventional CHP systems through enhanced energy conversion efficiency. With the global push for low-carbon energy transition, next-generation CHP technologies utilizing hydrogen-blended gas or pure hydrogen fuel are being developed. This advancement significantly boosts their strategic value in achieving carbon neutrality goals. Globally, CHP installed capacity continues to grow steadily, now accounting for over 30% of district heating systems in EU countries, making it an indispensable component of modern integrated energy systems.

CHP units in gas-fired thermal power plants generate both electricity and heat simultaneously. The power generation efficiency of CHP units refers to the proportion of total energy input from fuel converted into electrical energy[10].

$$P_{CHPe} = P_{CHPg} CHP_e \tag{10}$$

Where: P_{CHPe} , P_{CHPg} , CHP_e represents the CHP power generation capacity, the gas consumption power of CHP, and the power generation efficiency of the CHP unit.

Heating efficiency: The heating efficiency of a CHP unit is defined as the proportion of total energy input from fuel that is converted into thermal energy.

$$P_{CHPh} = P_{CHPg} CHP_h \tag{11}$$

P_{CHPh} represents the heat output of the CHP system, and CHP_h represents the thermal efficiency of the CHP.

Run Constraints:

$$\begin{cases} P_{CHP,down} \le P_{CHOg(t+1)} - P_{CHPg(t)} \le P_{CHP,UP} \\ P_{CHP,\min} \le P_{CHPg} \le P_{CHP,\max} \end{cases} \tag{12}$$

In the formula: $P_{CHP,down}$, $P_{CHP,UP}$ represent the upper and lower limits of the CHP unit's output power ramp rate, while, $P_{CHP,\min}$, $P_{CHP,\max}$ denote the upper and lower limits of the CHP unit's output power.

2.3 Modeling of Wind Power Output Uncertainty and Scenario Generation

2.3.1Joint probability model based on Copula function

Firstly, it is necessary to determine the univariate probability distribution of wind power and photovoltaic power output. In this paper, historical wind and solar power output data are utilized, and the non-parametric estimation method - Kernel Density Estimation (KDE) is employed to fit the marginal probability distribution function.

Compared with traditional parametric distributions (such as Weibull and Beta distributions), KDE does not require prior assumptions about the distribution form and can more flexibly capture the distribution characteristics of actual data. The marginal distribution function of wind and solar power output can be expressed by KDE as[11]:

$$\hat{f}_W(w) = \frac{1}{Nh_W}\sum_{i=1}^{N} K\left(\frac{w - W_i}{h_W}\right) \tag{13}$$

$$\hat{f}_P(p) = \frac{1}{Nh_P}\sum_{i=1}^{N} K\left(\frac{p - P_i}{h_P}\right) \tag{14}$$

W_i, P_i is a historical data sample, N represents the sample size, $K(\cdot)$ is the kernel function (in this case, a Gaussian kernel function is selected), h_W and h_P is the bandwidth parameter. The corresponding cumulative distribution function (CDF) can be obtained through integration.

Secondly, the Copula function is a function that connects the marginal distributions with the joint distribution, and can independently describe the correlation structure between variables. Considering that there exhibits asymmetrical tail correlations among the wind power outputs, this paper selects the Frank Copula, which performs well in describing the negative correlation between variables. Its distribution function can be expressed as[12]:

$$C_\theta(u,v) = -\frac{1}{\theta}\ln\left[1 + \frac{(e^{-\theta u} - 1)(e^{-\theta v} - 1)}{e^{-\theta} - 1}\right] \tag{15}$$

$u = F_W(w)$ $v = F_P(p)$ These are the marginal distribution values of wind power and photovoltaic power output. The parameters θ were obtained by fitting from historical data using the Maximum Likelihood Estimation (MLE) method. After establishing the joint probability model $F_{W,P}(w,p) = C_\theta(F_W(w), F_P(p))$, Monte Carlo Simulation is employed to generate a large number of initial random scenarios. The specific steps are as follows:

Step 1: Independently generate two uniform random variables q_1, q_2 from the interval [0, 1].

Step 2: Set $u = q_1$ and obtain v through the conditional distribution function $C_\theta(v \mid u)$ of the Frank Copula.

Step 3: Through the inverse operation of the marginal distribution, obtain the wind and solar power output scenario $(w,p) = (F_W^{-1}(u), F_P^{-1}(v))$.

2.3.2 Scene Reduction Based on K-means

K-means is an unsupervised clustering algorithm, aiming to divide N data points (here, the wind power output scene vector $\mathbf{s}_i = [w_i, p_i]$ into K clusters $\{C_1, C_2, ..., C_K\}$, such that the sum of the squared Euclidean distances from each data point to the center of its corresponding cluster is minimized[13]. Its objective function is:

$$J = \sum_{k=1}^{K}\sum_{\mathbf{s}_i \in C_k} \| \mathbf{s}_i - \boldsymbol{\mu}_k \|^2 \tag{16}$$

$\boldsymbol{\mu}_k$ is the center of cluster C_k.

Implementation steps: First, consider each initial scene $\mathbf{s}_i = (w_i, p_i)$ as a point in a two-dimensional space, and then initialize: randomly select K initial cluster centers $\{\boldsymbol{\mu}_1, \boldsymbol{\mu}_2, ..., \boldsymbol{\mu}_K\}$

Implementation steps: First, consider each initial scene as a point in a two-dimensional space. Then, initialize: randomly select K initial cluster centers. Iteration process: First, perform the allocation step: assign each scene $\mathbf{s}_i$ to the cluster center that is closest to it. The cluster c_i to which scene $\mathbf{s}_i$ belongs is determined by the following formula[14]:

$$c_i = \arg\min_k \| \mathbf{s}_i - \boldsymbol{\mu}_k \|^2 \tag{17}$$

The next step is to update: Recalculate the mean value for each cluster as the new cluster center:

$$\mu_k = \frac{1}{|C_k|}\sum_{s_i \in C_k} s_i \tag{18}$$

Convergence: Repeat the above two steps until the cluster centers no longer change significantly ($\| \mu_k^{new} - \mu_k^{old} \| < ò$) or the maximum number of iterations is reached.

Output: Eventually, K typical scenarios $\{S_1, S_2, ..., S_K\}$ are obtained, each represented by its cluster center μ_k. The probability π_k of each typical scenario is determined by the proportion of the initial scenarios contained within its cluster to the total number of scenarios[15].

$$\pi_k = \frac{N_k}{N} \tag{19}$$

N_k is the number of scenes in the K cluster.

The number of clusters K is a crucial parameter. In this paper, it is determined comprehensively through the Elbow Method in combination with the computational burden of the specific problem. The core idea of the Elbow Method is to observe the change curve of the within-cluster sum of squares (WCSS) under different K values, and select the K value corresponding to the turning point (i.e., the "elbow point") of the curve.

Through the above process, the uncertainty of wind power output is ultimately transformed into a discrete set containing several typical scenarios and their occurrence probabilities, laying a solid foundation for the stochastic optimal scheduling in the next chapter.

3. Market operation scheduling method based on Nash bargaining model

3.1 Cooperative Game Framework

We consider an alliance composed of three entities: a new energy power plant $i=1$, a gas-fired thermal power plant $i=2$, and a carbon capture plant $i=3$. The cooperation modes they can choose include independent operation or forming different forms of alliance.

The negotiation breakdown point: Let U_1^0, U_2^0, U_3^0 respectively represent the maximum benefits that the three parties can obtain when they do not cooperate and operate independently. This is the negotiation breakdown point in Nash bargaining, which is the minimum benefit requirement for all parties to participate in cooperation.

Total revenue of the alliance: Let denote the maximum total revenue U_{total} that can be obtained through optimal scheduling after the three of them form a large alliance and operate in coordination.

The basic premise of cooperation is that the total revenue of the alliance must be greater than the sum of the revenue of each member operating independently, that is, there is a cooperative surplus S [000006]:

$$S = U_{\text{total}} - (U_1^0 + U_2^0 + U_3^0) > 0 \tag{20}$$

3.2 Nash Bargaining Model

The Nash bargaining model seeks to establish a fair and efficient mechanism for distributing cooperative surplus. Its fundamental principle is that an equitable allocation scheme should maximize the product of all participants' utility relative to their bargaining breakdown points.

The Nash bargaining solution satisfies the following axioms: Pareto effectiveness, symmetry, affine transformation independence, and independence of irrelevant choices. Let x_1, x_2, x_3 be the benefits allocated to participants 1, 2, and 3 respectively after negotiation. The allocation scheme must satisfy[17]:

Individual rational constraint: the benefit received by each member is not less than his negotiation break point.

$$x_i >= U_i^0, i = 1,2,3 \tag{21}$$

Collective rationality constraint: total allocation equals total alliance revenue.

$$x_1 + x_2 + x_3 = U_{\text{total}} \tag{22}$$

Symmetric Nash Bargaining Solution In symmetric models (assuming all participants have identical bargaining power)[18], the Nash bargaining solution is obtained by solving the following Nash product maximization problem:

$$\max Z = (x_1 - U_1^0) \cdot (x_2 - U_2^0) \cdot (x_3 - U_3^0) \tag{23}$$

$$\text{s.t.} \quad \begin{cases} x_1 + x_2 + x_3 = U_{\text{total}} \\ x_1 \geq U_1^0, \quad x_2 \geq U_2^0, \quad x_3 \geq U_3^0 \end{cases} \tag{24}$$

Where $(x_i - U_i^0)$ represents the additional benefit obtained by the i-th participant from the cooperation.

By constructing the Lagrange function L and finding the first-order optimality conditions, the optimal distribution can be obtained as follows :

$$x_1 - U_1^0 = x_2 - U_2^0 = x_3 - U_3^0 \tag{25}$$

This means that the cooperative surplus is evenly distributed among all participants. The final payoff for each participant is:

$$x_i = U_i^0 + \frac{S}{3} = U_i^0 + \frac{U_{\text{total}} - (U_1^0 + U_2^0 + U_3^0)}{3} \tag{26}$$

Asymmetric Nash Bargaining Solution (with Weighting Factor)

In practical applications, varying investment scales, risk exposures, and technological significance among participants result in differing bargaining power. To address this, a weighting factor α_i ($\alpha_i > 0$ and $\alpha_1 + \alpha_2 + \alpha_3 = 1$) is introduced to represent each party's relative bargaining capacity. This article combines the resource input, operational risk, and technological contribution of three parties, and uses the AHP method to determine the weight factors: investment cost (40%), operational risk (30%), and technological contribution (30%) are used as evaluation criteria, and the final weight combination is $\alpha_1 = 0.25$ (new energy power plant), $\alpha_2 = 0.35$ (gas-fired thermal power plant), and $\alpha_3 = 0.40$ (carbon capture power plant), which satisfies $\alpha_1 + \alpha_2 + \alpha_3 = 1$. The selection criteria are as follows: carbon capture power plants have the highest weight due to the large investment scale of CCS and P2G equipment and the high risk of low-carbon technology; The technology of CHP units in gas-fired thermal power plants is mature, with balanced investment and risk, and a moderate weight; New energy power plants mainly rely on wind and solar power generation, with relatively low investment and slightly lower weight. This combination can objectively reflect the actual participation value of all parties in the alliance. The generalized Nash product is then defined as[19]:

$$\max Z = (x_1 - U_1^0)^{\alpha_1} \cdot (x_2 - U_2^0)^{\alpha_2} \cdot (x_3 - U_3^0)^{\alpha_3} \tag{27}$$

$$\text{s.t.} \quad \begin{cases} x_1 + x_2 + x_3 = U_{\text{total}} \\ x_1 \geq U_1^0, \quad x_2 \geq U_2^0, \quad x_3 \geq U_3^0 \end{cases} \tag{28}$$

To solve this optimization problem, we obtain the asymmetric Nash bargaining solution, which satisfies:

$$\frac{x_1 - U_1^0}{\alpha_1} = \frac{x_2 - U_2^0}{\alpha_2} = \frac{x_3 - U_3^0}{\alpha_3} \quad (29)$$

At this point, the remaining allocation of cooperation is proportional to the weight factor[20]. The final payoff for each participant is:

$$x_i = U_i^0 + \alpha_i \cdot S = U_i^0 + \alpha_i \cdot \left[U_{\text{total}} - (U_1^0 + U_2^0 + U_3^0) \right] \quad (30)$$

Weight factors can be determined through various methods, such as investment cost ratio, risk coefficient, or AHP (Analytic Hierarchy Process) method.

3.3 Two-stage optimization solution process

The first stage is the optimization scheduling of the alliance. This stage aims to determine the optimal operation strategies and corresponding revenues under different alliance structures, and its core objective is to calculate the total revenue of the large alliance U_{total}. This problem is a complex mixed-integer linear programming problem, and its mathematical model is based on all the constraints and objective functions established in Chapter 2. The objective function is as follows[21]:

$$\max U_{\text{total}} = \sum_{t=1}^{T} \left[R_e(t) + R_h(t) + R_g(t) - C_{\text{fuel}}(t) - C_{\text{oM}}(t) - C_{\text{curt}}(t) \right] \quad (31)$$

T : Dispatch cycle (24 hours)

$R_e(t)$: Electricity revenue at time t, $R_e(t) = \lambda_e(t) \cdot P_{sell}(t)$

$R_h(t)$: Heating revenue at time t, $R_h(t) = \lambda_h(t) \cdot Q_{sell}(t)$

$R_g(t)$: Gas revenue at time t, $R_g(t) = \lambda_g(t) \cdot G_{sell}(t)$

$C_{\text{fuel}}(t)$: Fuel cost at time t

$C_{\text{oM}}(t)$: Operation and maintenance cost at time t

$C_{\text{curt}}(t)$: Penalty cost for wind and solar power curtailment at time t.

The power balance constraints, heat power balance constraints and gas power balance constraints are as follows[18-19].This constraint ignores the transmission loss of the power grid and is applicable to scenarios where multiple entities collaborate closely within a regional level integrated energy system - new energy power plants, gas-fired thermal power plants, and carbon capture power plants in alliances are geographically concentrated, with short transmission distances (usually not exceeding 50km) and actual transmission losses accounting for only 2% -3%, which belongs to the category of engineering negligible

$$P_{\text{wind}}(t) + P_{\text{pv}}(t) + P_{\text{CHP}}(t) + P_{\text{grid,buy}}(t) = P_{\text{load}}(t) + P_{\text{P2G}}(t) + P_{\text{grid,sell}}(t) \quad (32)$$

$$Q_{\text{CHP}}(t) + Q_{\text{gas-boiler}}(t) = Q_{\text{load}}(t) + Q_{\text{heat,sell}}(t) \quad (33)$$

$$G_{\text{gas,well}}(t) + G_{\text{P2G}}(t) + G_{\text{grid,buy}}(t) = G_{\text{CHP}}(t) + G_{\text{gas-boiler}}(t) + G_{\text{load}}(t) + G_{\text{gas,sell}}(t) \quad (34)$$

Phase 2: Nash Bargaining Interest Allocation. Using the optimized parameters U_{total}, U_i^0 from Phase 1 as inputs, we apply the Nash bargaining model established in this chapter to solve the problem. Input: U_{total}, U_1^0, U_2^0, U_3^0 weight factor α_i. weight factors. Model: Select either a symmetric or asymmetric model based on whether to account for differences in bargaining power. Output: Fair interest allocation scheme x_1, x_2, x_3.

Symmetric Nash Bargaining Model[22]:

$$\max Z = (x_1 - U_1^0) \cdot (x_2 - U_2^0) \cdot (x_3 - U_3^0) \quad (35)$$

$$\begin{cases} x_1 + x_2 + x_3 = U_{\text{total}} \\ x_1 \geq U_1^0, x_2 \geq U_2^0, x_3 \geq U_3^0 \end{cases} \quad (36)$$

Asymmetric Nash Bargaining Model[23]:

$$\max Z = (x_1 - U_1^0)^{\alpha_1} \cdot (x_2 - U_2^0)^{\alpha_2} \cdot (x_3 - U_3^0)^{\alpha_3} \quad (37)$$

$$\begin{cases} x_1 + x_2 + x_3 = U_{\text{total}} \\ x_1 \geq U_1^0, x_2 \geq U_2^0, x_3 \geq U_3^0 \end{cases} \quad (38)$$

The two-stage method ensures the economic optimality of operation scheduling and the fairness and rationality of benefit distribution, thus forming a market operation scheme that can motivate all subjects to participate actively and maintain the stable operation of the alliance.

4. Computational analysis of examples

The case study is based on the actual operation data of a regional power grid in Liaoning Province, China. It covers the daily load curves of electricity, heat, hydrogen and gas, as well as time-of-use electricity prices and gas prices, and historical data of wind and solar power generation. The key equipment parameters of the system include: the rated capacity of the wind farm is 80 MW, the photovoltaic power station is 50 MW, the maximum hydrogen production power of the P2G electrolyzer is 20 MW, the efficiency of the methane reactor is 0.65, the capacity of the hydrogen storage tank is 120 MWh, the heat-to-electricity ratio of the CHP unit is 1.2, and the CO_2 capture rate of the carbon capture power plant is 90%. In terms of cost parameters, the penalty cost for lost wind or solar power is 0.15 RMB/kWh, the purchase price of natural gas is 2.8–4.2 RMB/m³, and the purchase price of electricity from the grid is 0.3–0.9 RMB/kWh. The optimization scheduling period is 24 hours, with a time step of 1 hour, and the Gurobi solver is used for solving the mixed integer linear programming.

4.1 Model input basic data analysis

The 24-hour load data and energy prices in a certain region of Liaoning Province are shown in Figure 2 and Figure 3.

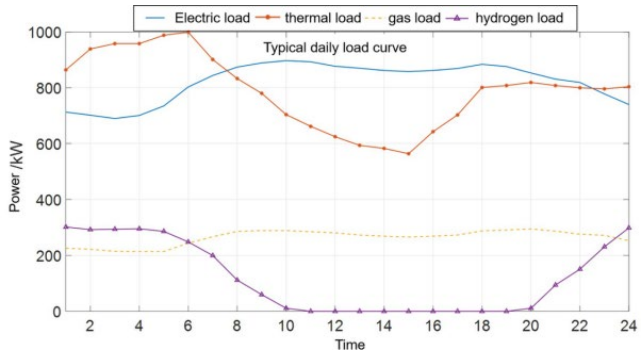

Figure 2. Typical daily load curve

The region experiences peak electricity demand from 6:00 AM to 10:00 PM, with significant daily fluctuations likely linked to industrial or residential peak hours. Thermal load peaks between 6:00 PM and 8:00 AM the next day, mirroring daily routines. Hydrogen demand emerges between 8:00 PM and 10:00 AM the following day, concentrated in specific periods, possibly for hydrogen refueling of fuel cell vehicles or industrial applications. Gas consumption remains relatively evenly distributed throughout the day, likely supporting continuous industrial processes or basic gas supply needs.

Figure 3. Daily gas/electricity purchase price

The region experiences higher gas purchase prices between 6:00 AM and 5:00 PM, as well as between 8:00 PM and 11:00 PM, with overall gas supply remaining stable due to pipeline capacity constraints. Electricity prices are higher from 7:00 AM to 9:00 PM. During off-peak hours, facilities like P2G systems convert excess electricity into gas, reducing electricity purchases during peak demand periods. Utilizing P2G technology during low-cost electricity periods lowers production costs, while minimizing purchases during high-demand times. This strategy prioritizes renewable energy sources or activates CHP systems to ensure stable energy supply. The photoelectric output and wind power output of this paper are shown in Figure 4 and Figure 5.

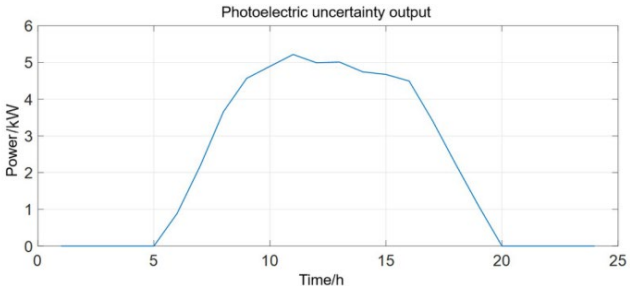

Figure 4. Photoelectric uncertainty output

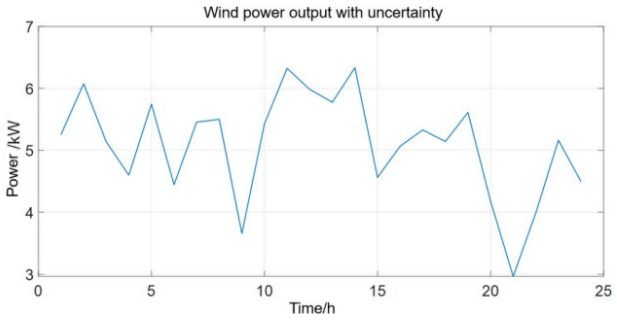

Figure 5. Wind power output with uncertainty

The region generates photovoltaic power from 5 a.m. to 8 p.m., which helps avoid solar curtailment and maximizes energy utilization. Wind power output in this area fluctuates significantly, and equipment like P2G can also reduce wind curtailment.

4.2 Optimization result analysis

The new energy power plant is F_1, the gas-fired thermal power plant is F_2, and the carbon capture power plant is F_3. F_{123} is the new energy power plant, gas-fired thermal power plant, and carbon capture power plant operate in cooperation.

Figure 6-7 illustrates the system power load balance for F_{123}, F_{12}.

During the 08:00–12:00 period, the combined output of wind power and photovoltaic power reached 110–130 MW, meeting approximately 70% of the load demand; the CHP units increased their output to 45 MW during the peak electricity price period (such as 10:00), effectively reducing the cost of purchased electricity; P2G absorbed approximately 15 MW of surplus wind power during the low electricity price period (02:00 – 05:00) at night, achieving the transfer of energy across time periods.

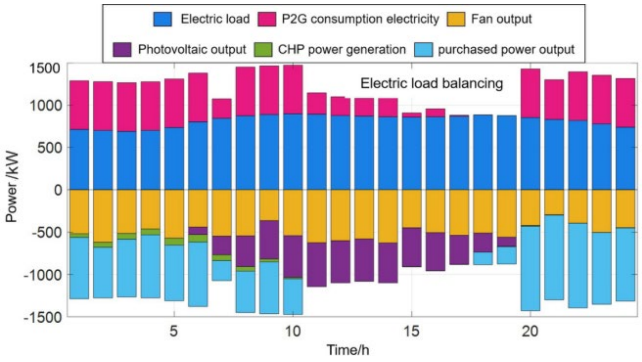

Figure 6. F_{123} System electrical load balance

Due to the lack of new energy power sources, the system's purchased power during peak daytime hours (such as 11:00) reached as high as 85 MW, an increase of approximately 40% compared to the tripartite alliance model, resulting in a 28% rise in the total purchased power cost.

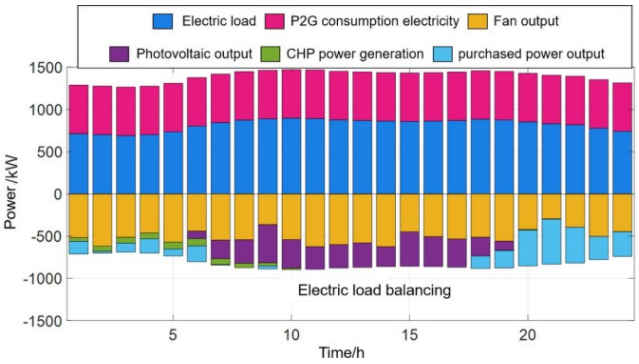

Figure 7. F_{12} System electrical load balance

The gas-fired thermal power plant and carbon capture power plant operate in a collaborative system without participation from new energy plants. The gas-fired plant provides CHP units for combined heat and power generation, while the carbon capture plant runs P2G equipment and hydrogen storage tanks to achieve cross-temporal energy storage. Without new energy plants, the system must rely entirely on grid electricity and CHP power purchases. Due to the ramping-up limitations of CHP units and hydrogen storage tanks, the overall flexibility is lower than that of the three-party alliance. The total power procurement cost remains extremely high due to the absence of wind and solar power supply.

Figure 8-9 shows the system gas load balance for F_{123} , F_{12} . During the low-price period of electricity (03:00–06:00), P2G generates hydrogen with a power output of 18 MW, replacing a portion of the purchased natural gas. During the peak gas price period (18:00–20:00), the CHP units reduce gas consumption, resulting in a total reduction of approximately 15% in the system's gas consumption cost.

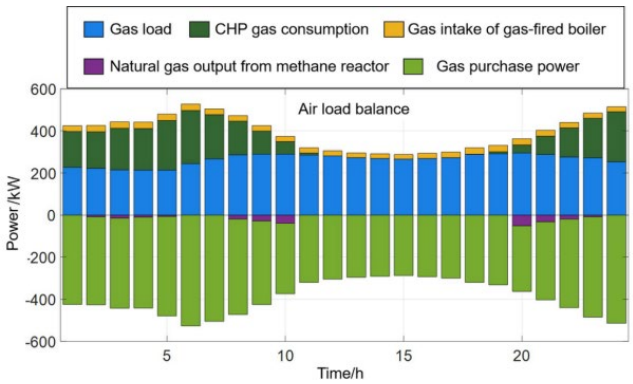

Figure 8. F_{123} System gas load balance

Due to the inability to utilize new energy sources to regulate the P2G operation, the hydrogen production volume of the system is limited during the low-price period of electricity, resulting in an increase of 12% in gas consumption costs compared to the three-party alliance model, and a decrease in overall operational flexibility.

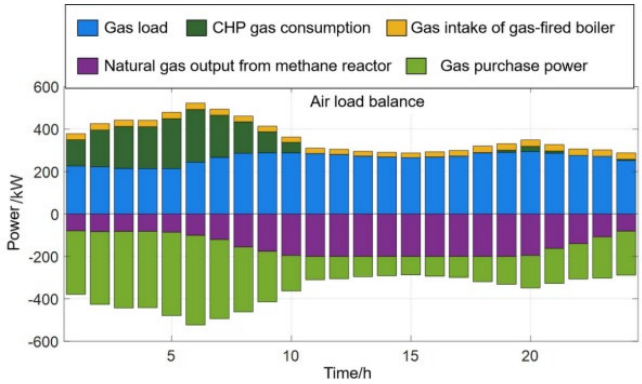

Figure 9. F_{12} System gas load balance

The absence of new energy power plants prevents the regulation of P2G equipment operations based on renewable energy. During off-peak electricity periods, the P2G system operates at high capacity, consuming large amounts of low-cost electricity for energy storage. Meanwhile, CHP systems reduce power output, leading to decreased gas purchases. During peak electricity periods, P2G equipment shuts down while CHP systems ramp up to minimize electricity purchases, resulting in increased external gas procurement. However, the overall alliance still faces rising electricity costs and diminished benefits due to the lack of new energy power plants participation.

4.3 The result of the benefit distribution

The collaborative Shapley value distribution results are shown in Table 1.

Table 1. Shapley value distribution comparison before and after

Participants	Independent operating income(RMB)	Cooperative Shapley value allocation (RMB)
New energy power plant	14956.86	15225.38
Gas-fired thermal power plant	1652.95	2916.35

The allocation results satisfy: individual rationality, meaning each participant's share is no less than their independent operation benefit; collective rationality, ensuring the total allocation equals the grand alliance's benefit; and incentive compatibility, motivating all participants to cooperate.

In conclusion, compared with the independent operation mode, the tripartite alliance (S1 + S2 + S3) achieves a reduction of approximately 22% in the total system operation cost through the coordinated optimization of electric, thermal, gas, and hydrogen multi-energy flows. At the same time, the renewable energy consumption rate has increased by 18%. Moreover, the benefit distribution scheme achieved through the Nash bargaining mechanism not only satisfies individual rationality and collective rationality, but also reflects the differences in investment and risks among all parties, effectively ensuring the stability and cooperation enthusiasm of the alliance.

5. Research conclusions

This paper constructs an optimization scheduling model for a comprehensive energy system integrating renewable energy, gas-fired thermal power, and carbon capture power plants, and designs a cooperative residual allocation mechanism based on the Nash bargaining theory. The results of the case study (as detailed in Section 4.2) demonstrate that the three-party alliance model, through collaborative optimization of multi-energy flows, achieves significant improvements in both economic performance and renewable energy utilization compared to independent operation.In terms of benefit distribution, the proposed Nash bargaining mechanism successfully distributes the total cooperative revenue fairly among all participating entities. The distribution results not only satisfy individual rationality and collective rationality, but also reflect the differences in investment and risks among all parties, thereby effectively ensuring the stability and cooperation enthusiasm of the alliance. Moreover, the introduction of hydrogen energy storage and P2G technology significantly enhances the multi-energy complementarity and cross-time regulation capabilities of the system, providing key technical support for the consumption of high proportions of renewable energy. For example, the example shows that P2G can absorb about 15MW of wind power surplus during the low electricity price period at night, convert it into natural gas, and replace about 12% of external gas purchases during the peak gas price period during the day. This specifically reflects the multi energy complementarity and cost saving benefits achieved by this technology through energy spatiotemporal transfer. This research provides theoretical basis and method references for the collaborative operation and market-oriented trading of multi-party participation in comprehensive energy systems. Future work can introduce interdisciplinary theories such as economics to further improve the allocation mechanism and expand the generation method considering seasonal characteristics to enhance the universality of the model.

Acknowledgements.

This paper is supported by “State Grid Jilin Electric Power Co., Ltd. 2025 High-Quality Development Strategic Research Project Funding” (Project No. SGJLJY00ZLJS2500042).

References

[1] Duch-Brown N, Rossetti F. Digital platforms across the European regional energy markets[J]. Energy Policy, 2020, 144: 111612.

[2] Singh A R, Kumar R S, Bajaj M, et al. A blockchain-enabled multi-agent deep reinforcement learning framework for real-time demand response in renewable energy grids[J]. Energy Strategy Reviews, 2025, 62: 101905.

[3] Mansouri S A, Nematbakhsh E, Ramos A, et al. A robust ADMM-enabled optimization framework for decentralized coordination of microgrids[J]. IEEE Transactions on Industrial Informatics, 2024.

[4] Jørgensen B N, Ma Z G. Digital Twin of the European Electricity Grid: A Review of Regulatory Barriers, Technological Challenges, and Economic Opportunities[J]. Applied Sciences, 2025, 15(12): 6475.

[5] Jacob E., Farzaneh H. Modeling and performance evaluation of hybrid photovoltaic thermal, wind, and battery microgrids using optimization and dynamic simulation. Sci Rep 15, 11528 (2025).

[6] Zhang H, Zandehshahvar R, Tanneau M, et al. Weather-informed probabilistic forecasting and scenario generation in power systems[J]. Applied Energy, 2025, 384: 125369.

[7] Abdallah R Y, Shaaban M F, Osman A H, et al. Synergizing Gas and Electric Systems Using Power-to-Hydrogen: Integrated Solutions for Clean and Sustainable Energy Networks[J]. Smart Cities, 2025, 8(3): 81.

[8] Gui L. A Market-Based Mechanism for Global Vaccine Procurement Coalitions[J]. Manufacturing & Service Operations Management, 2025.

[9] Foglia K R, Pisani F S, Colao V. Limited Memory LRSGA Optimizer to competitive optimization[J]. arXiv preprint arXiv:2510.26983, 2025.

[10] Li, Y., Wang, C., and Zhang, Q. Stackelberg-Nash bargaining-based low-carbon scheduling for multiple integrated multi-energy systems. Energy, vol. 295, p. 131015, 2025.

[11] Yang J, Liang T, Mi D, et al. Low-carbon optimization scheduling of a CCS-P2G-HFC integrated energy system with 2D-DR under multi-mechanism collaboration[J]. Energy, 2025: 138348.

[12] Chen, S., and Li, P. Equilibrium allocation strategy of distributed ESSs balancing ecology and economics in DNs

considering carbon taxation systems. Applied Energy, vol. 362, p. 123001, 2025.
[13] Lu P, Li J, Liu S, et al. Hierarchical reserve-based distributionally robust chance-constrained optimization for integrated electricity-heat systems during cold waves[J]. Applied Energy, 2026, 402: 126900.
[14] Zheng B, Wei W, Xu Y, et al. Capacity aggregation and online control of clustered energy storage units[J]. IEEE Transactions on Sustainable Energy, 2024, 15(3): 1546-1561.
[15] Wang, M., Li, J., and Zhang, W. An Optimal Operation Strategy for Multi-Microgrid Cooperative Game Considering Energy Trading Based on Nash Bargaining Model. Power System Protection and Control, vol. 52, no. 10, pp. 1-12, 2024.
[16] Liu. J., Duan. L., Chen. J., et al. A Cooperative Operation Strategy for Multi-Energy Systems Based on Nash Bargaining. Electronics, vol. 13, no. 15, p. 3015, 2024.
[17] Micheli G, Escudero L F, Maggioni F, et al. Multi-horizon optimization for domestic renewable energy system design under uncertainty[J]. arXiv preprint arXiv:2505.15167, 2025.
[18] Emdadi K, Gandomkar M, Nikoukar J. Adaptive Robust Energy Management of Smart Grid with Renewable Integrated Energy System, Fuel Cell and Electric Vehicles Stations and Renewable Distributed Generation[J]. Results in Engineering, 2025: 106857.
[19] Jia Q, Zhang T, Zhu Z, et al. Harnessing hydrogen energy storage for renewable energy stability in China: A path to carbon neutrality[J]. International Journal of Hydrogen Energy, 2025, 118: 93-101.
[20] Salman M, Kashif S A R, Fakhar M S, et al. Optimizing power generation in a hybrid solar wind energy system using a DFIG-based control approach[J]. Scientific Reports, 2025, 15(1): 10550.
[21] Meng Q, He Y, Hussain S, et al. Low carbon optimization for wind integrated power systems with carbon capture and energy storage under carbon pricing[J]. Scientific Reports, 2025, 15(1): 32714.
[22] Liu, D., Chen, H., and Zhou, R. A Multi-Time Scale Cooperative Operation Optimization Model for Electricity-Hydrogen Energy System Based on Nash Bargaining. Proceedings of the CSEE[J]. vol. 44, no. 1, pp. 100-113, 2024.
[23] Hu Y, Wu Z, Ding Y, et al. Optimal Energy Management and Trading Strategy for Multi-Distribution Networks with Shared Energy Storage Based on Nash Bargaining Game[J]. Processes, 2025, 13(7): 2022.